ACS APPLIED MATERIALS & INTERFACES

Letter

www.acsami.org

In Situ Growth of MOFs on the Surface of Si Nanoparticles for Highly Efficient Lithium Storage: Si@MOF Nanocomposites as Anode Materials for Lithium-Ion Batteries

Yuzhen Han,[†,⊥] Pengfei Qi,[†,⊥] Xiao Feng,[†] Siwu Li,[†] Xiaotao Fu,[†] Haiwei Li,[†] Yifa Chen,[†] Junwen Zhou,[‡] Xingguo Li,[‡] and Bo Wang*[,†]

[†]Key Laboratory of Cluster Science, Ministry of Education of China, School of Chemistry, Beijing Institute of Technology, 5 South Zhongguancun Street, Beijing 100081, P.R. China

[‡]College of Chemistry and Molecular Engineering, Peking University, 5 Yiheyuan Road, Beijing 100871, P.R. China

Supporting Information

ABSTRACT: A simple yet powerful one-pot strategy is developed to prepare metal−organic framework-coated silicon nanoparticles via in situ mechanochemical synthesis. After simple pyrolysis, the thus-obtained composite shows exceptional electrochemical properties with a lithium storage capacity up to 1050 mA h g^{-1}, excellent cycle stability (>99% capacity retention after 500 cycles) and outstanding rate performance. These characteristics, combined with their high stability and ease of fabrication, make such Si@MOF nanocomposites ideal alternative candidates as high-energy anode materials in lithium-ion batteries.

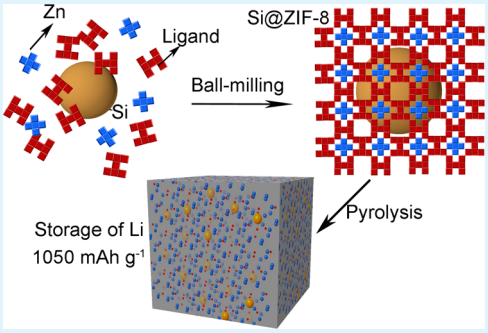

KEYWORDS: *metal−organic framework, energy, lithium storage, silicon, in situ growth*

With the prosperity of society and economy, exploring new and clean energy is becoming increasingly urgent. Lithium-ion battery (LIB) has been developed as one of the most important devices for electrochemical energy storage.[1,2] The new active electrode materials with high capacity and long cycle life are highly desired yet the need is largely unmet. Metal−organic frameworks (MOFs) are porous materials assembled by joining metal ions with preferable organic linkers. In the past decades, great efforts have been focused on preparing new MOF structures and exploiting their applications, including gas storage and separation, catalysis, sensing, and drug delivery.[3] Yet the application on Li storage is burgeoning. Some pioneering work has been done in using MOFs for energy storage, such as supercapacitors,[4] energy storage materials,[5] LIBs,[6] etc. Particularly, several MOFs, such as MOF-5,[7] MOF-199,[8] MIL-88,[9] and ZIF-8,[10] have been utilized as the anode materials in LIBs.[11] Coincidentally, we had recently introduced two distinct approaches to develop active electrode materials using MOFs: (1) encapsulating sulfur molecules inside MOF cavities with proper size and functionalities for Li−S batteries[12] and (2) pyrolysis of MOFs to obtain carbon frameworks with monodispersed metal centers as the anode materials.[10] Nevertheless, the limited capacity, low Coulombic efficiency, or cycle stability of these MOF-based electrode materials makes them unsatisfactory for industrial applications.

Silicon is a promising anode material[13] because of its high theoretical capacity of 4200 mA h g^{-1}. However, the use of Si as anode material in LIBs suffered from the rapid capacity decay during the cycling because of its up to ∼300% volume change. Hence, finding ways to protect Si from undesired swelling−shrinking and then keeping the close contact of the conductive species and the electrolyte of Si is of great importance.[14] Many research groups have contributed in this field, and some prime examples include fabrication of different forms of Si nanostructures[15] and surface modification of Si by carbon[16] or metal[17] coating. However, the exceedingly complicated and very expensive method is always the limited reason for mass production.

The construction of specific configuration of composites with homogeneous encapsulation of Si nanostructures into MOF-derived carbon matrix may have major advantages. First, the embedded Si nanoparticles can provide high capacity and the MOFs matrix can effectively mitigate the volume change of Si. Second, the porous carbon framework with uniformly distributed metal centers is beneficial for improving conductivity and further enhances the storage capacity. Third, the inherent open channels in the matrix are favorable for the transportation of Li^+ and facilitate rate performance.

Herein, we introduce a one-pot method to assemble MOFs on the surface of nano Si (denoted as Si@ZIF-8) by simply

Received: November 21, 2014
Accepted: January 9, 2015
Published: January 9, 2015

DOI: 10.1021/am5081937
ACS Appl. Mater. Interfaces 2015, 7, 2178−2182

grinding the MOF starting materials (metal salts and ligands) along with silicon nanoparticles with the addition of solvent initiator. Subsequently, thus-obtained composite is further carbonized and tested as the active anode materials (Figure 1). Si@ZIF-8 is pyrolyzed at 700 °C for 1 h at nitrogen

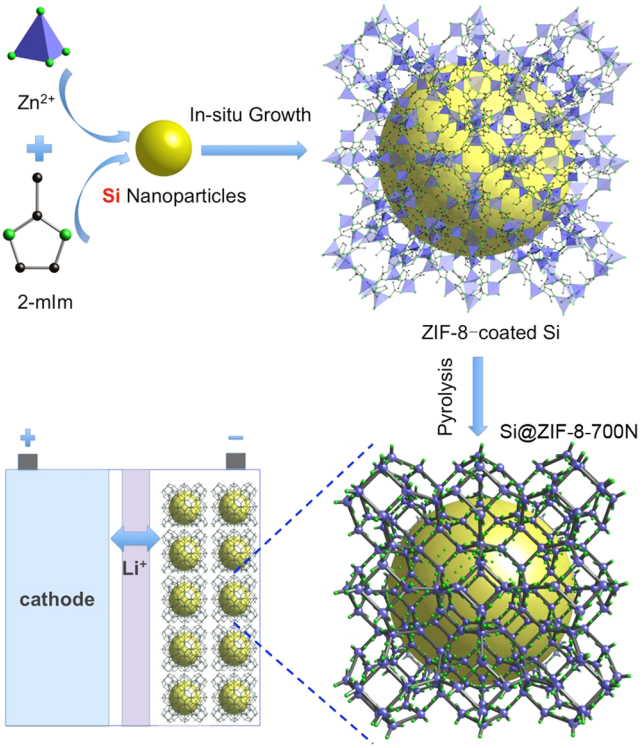

Figure 1. Schematic representation of the preparation of Si@ZIF-8-700N for anode material in LIBs. Color code: carbon, black; nitrogen, green; zinc, blue; silicon, yellow. After pyrolysis, ZIF-8 converts to amorphous carbon with monodispersed zinc ions.

atmosphere (denoted as Si@ZIF-8-700N). The capacity of the material can reach 1050 mA h g^{-1} (calculated by the active materials Si@ZIF-8-700N) and remain stable for more than 500 charge–discharge cycles; the high initial Coulombic efficiency benefits from the homogeneous encapsulation of Si. (Detailed experimental procedures can be found in the experimental section in the Supporting Information.)

The powder X-ray diffraction (PXRD) pattern of Si@ZIF-8 resembles those of both ZIF-8 and Si (Figure 2a). After pyrolysis, all the peaks assigned to ZIF-8 disappeared, whereas the peaks attributed to the crystalline Si were retained. The three main diffraction peaks at 28.5, 47.4, and 56.3° in the diffraction patterns of Si@ZIF-8-700N are ascribed to the (111), (220), and (331) facets of Si, respectively. It can be concluded that the skeleton of ZIF-8 after pyrolysis is collapsed and formed amorphous Zn, N and carbon composites. To verify this, Si@ZIF-8-700N was characterized by elemental analysis. The elemental composition of Si@ZIF-8-700N from inductively coupled plasma atomic emission spectrometer (ICP) and elemental analysis are summarized in Table S1 in the Supporting Information. It shows that the weight content of Zn and Si is 30.7% and 7.3%, respectively. The molar ratio is 1.8:1, which is close to the starting molar ratio 2:1. The total content of Zn, Si, C, N, and H elements is 99.9%. XPS and EDX show lower contents of Zn and Si (see Table S1 in the Supporting Information), because most of the Zn and Si are

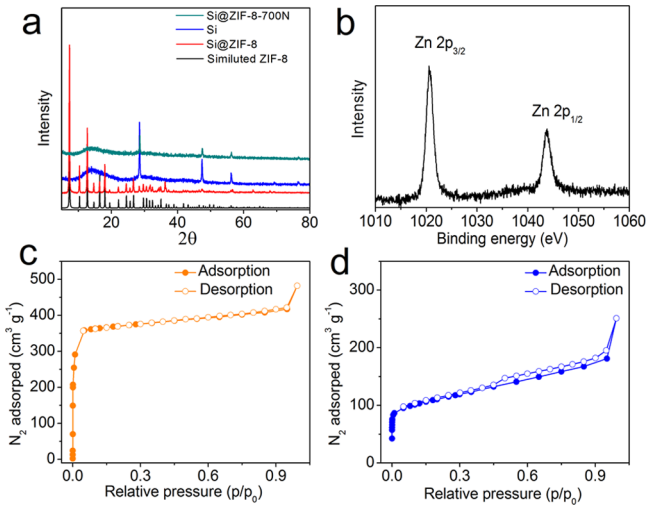

Figure 2. (a) PXRD patterns of Si@ZIF-8 and Si@ZIF-8-700N. (b) XPS spectra of Zn 2p for Si@ZIF-8-700N. (c, d) Nitrogen sorption isotherms of (c) Si@ZIF-8 and (d) Si@ZIF-8-700N at 77 K. "700N" denotes a sample heated at 700 °C under nitrogen atmosphere for 1 h.

located in the inner area of the materials. The XPS spectrum of Si@ZIF-8-700N (Figure 2b) exhibits two peaks assignable to Zn $2p_{3/2}$ (1020.5 eV) and Zn $2p_{1/2}$ (1043.7 eV), respectively. The Zn $2p_{3/2}$ line has been shifted by ΔE_{Zn} = 1 eV from the binding energy position of 1021.5 eV for elemental zinc,[18] suggesting the possible binding of zincs to form Zn–N.[19] The amorphous carbon matrix in Si@ZIF-8-700N (see Figure S1b in the Supporting Information) is constructed by C–C, C–N, and C–Si bonds. The XPS of N 1s (see Figure S1c in the Supporting Information) shows that N is present in the forms of N–C, N–Zn, N–H, and N–Si. The Si 2p peak is not visible (see Figure S1d in the Supporting Information), indicating that Si is fully coated with a thickness exceeding the depth of XPS analyses (~10 nm).

The nitrogen sorption isotherms and pore size distributions of Si@ZIF-8 and Si@ZIF-8-700N are shown in Figure 2c, d and Figure S2a, b in the Supporting Information. Si@ZIF-8 has a Brunauer–Emmett–Teller (BET) specific surface area of 1070 m^2 g^{-1} and a narrow pore size distribution around 1 nm. The reason for the lower surface area than ZIF-8 is the encapsulated Si (the nitrogen sorption isotherms and pore size distributions of pure nano Si are shown in Figure S3 in the Supporting Information). The pore size distribution of the composites coincides with the pore size of ZIF-8. These results together with TEM measurement suggest that MOFs are covered on the surface of Si rather than that silicon nanoparticles are embedded in the micropores of ZIF-8. The average pore size of ZIF-8 is about 1.1 nm. Therefore, Si NP with the size of 30–100 nm cannot enter the micropores of ZIF-8. Furthermore, the pore size distribution of Si@ZIF-8 is similarly as that of ZIF-8 (c.a., 1.1 nm), which confirmed that the micropores of Si@ZIF-8 are remained and not occupied by Si NP. The TEM images (Figure S4d in the Supporting Information) also show that the Si nanoparticles are embedded in ZIF-8 rather than in the micropores of ZIF-8. After pyrolysis, the specific surface area dramatically drops to 351 m^2 g^{-1}, and the mesopores of 2–10 nm are generated in Si@ZIF-8-700N. The generation of mesopores after pyrolysis is due to the collapse of the skeletons and partially vaporized sites. It has been proved that proper surface areas and the formation of

DOI: 10.1021/am5081937
ACS Appl. Mater. Interfaces 2015, 7, 2178–2182

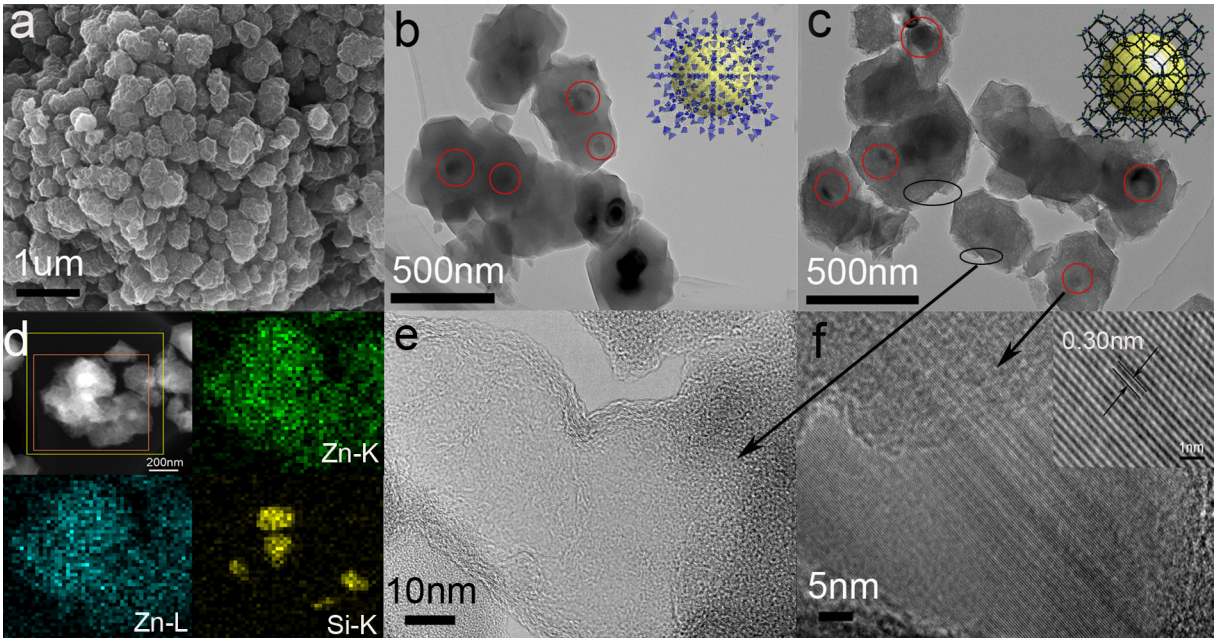

Figure 3. (a) SEM image of Si@ZIF-8-700N. (b) TEM image of Si@ZIF-8. The round balls embedded in the material are Si (50−100 nm). (c) TEM image of Si@ZIF-8-700N. After pyrolysis, ZIF-8 converts to amorphous carbon with well-dispersed zinc ions. (d) Elemental mapping of Si@ZIF-8-700N for Zn and Si by energy-dispersive X-ray spectroscopy (EDS). Si nanoparticles are completely wrapped by ZIF-8-derived composites (e) HRTEM image of the edge of Si@ZIF-8-700N (black circles). (f) HRTEM image of the center of Si@ZIF-8-700N (red circles).

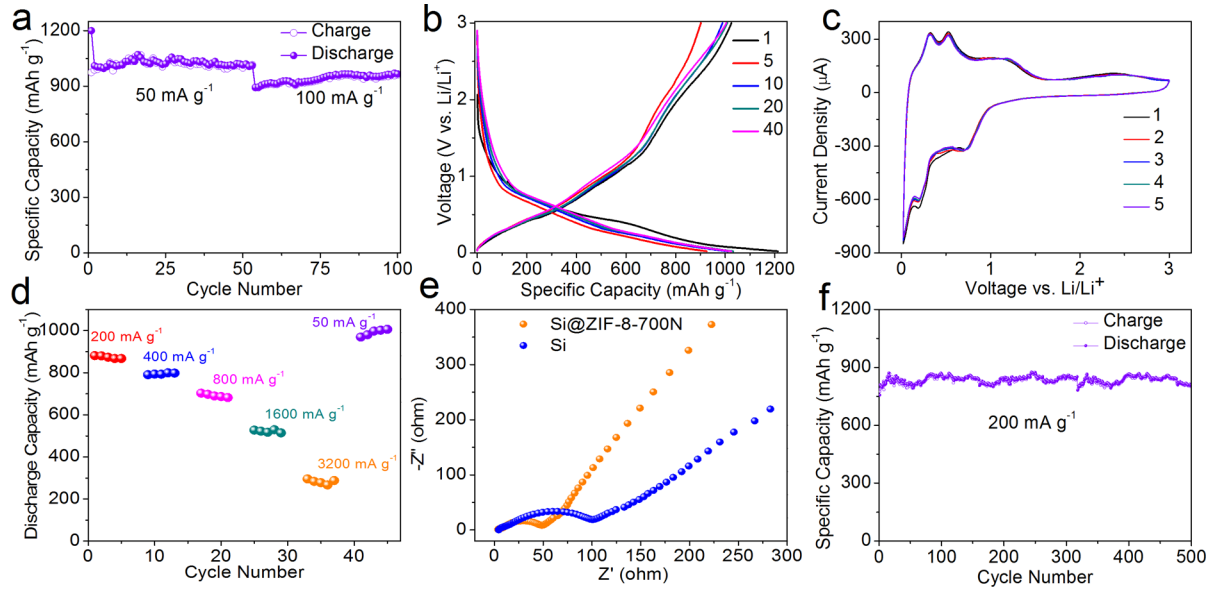

Figure 4. (a) Cycling performance of Si@ZIF-8-700N. (b) Voltage profile of Si@ZIF-8-700N. (c) Cyclic voltammetry measurements on Si@ZIF-8-700N after 4-cycles activating of the cell. The voltage range is 20 mV to 3.0 V at a scan rate of 0.1 mV s^{-1}. The initial point corresponded to the open-circuit voltage of the cell. (d) Discharge capacity of Si@ZIF-8-700N at various current densities. The cells were cycled for 10 times at a current density of 50 mA g^{-1} before the test. The current density varies from 200 to 3200 mA g^{-1}. (e) Nyquist plots for Si@ZIF-8-700N and nano Si after four cycles. (f) Long cycle performance of Si@ZIF-8-700N at 200 mA g^{-1}.

mesoporous nanostructures are favorable for lithium anode materials.[20−22]

The morphology and microstructure of these composites are examined through scanning electron microscope (SEM) and high-resolution transmission electron microscopy (HRTEM). The EM image of Si@ZIF-8 reveals that the sample is consisted of aggregated nanoparticles with diameters of 250 nm (see Figure S4b in the Supporting Information). Transformation of the nanoparticles with smooth surface into agglomerated clusters with irregular morphology is noted after the pyrolysis of primitive Si@ZIF-8 at 700 °C for 1 h (Figure 3a). The particles that are reunited together have the property of ball-milled ZIF-8. The size of different single granule is of varying sizes. The HRTEM images demonstrate that the sphere-shaped Si with the diameter of 50−100 nm is fully covered by ZIF-8 (Figure 3b) and carbonized ZIF-8 (Figure 3c). Clear crystal planes with a *d*-spacing of 0.23 nm can be found in the HRTEM image of Si@ZIF-8 (see Figure S4d in the Supporting

DOI: 10.1021/am5081937
ACS Appl. Mater. Interfaces 2015, 7, 2178−2182

Information), which corresponds to the (220) planes of crystalline Si. On the other hand, no obvious lattice fringes are observed in the coating layers around the Si particles, which are expected because pure ZIF-8 shows no lattice fringes under the same conditions. After pyrolysis, clear crystal planes with a *d*-spacing of 0.30 nm can be found in the HRTEM image of Si@ZIF-8-700N (Figure 3f), corresponding to the (111) planes of crystalline Si. At the edge of Si@ZIF-8-700N, layers of graphitic carbon are formed, which are beneficial for the promotion of electrical conductivity. Energy-dispersive X-ray spectroscopy (EDX) is utilized to map Si and Zn. Zn is uniformly distributed in the material, while Si is located in the inner areas. This result confirmed that Si nanoparticles are completely wrapped by ZIF-8-derived composites (Figure 3d).

The advantages of the present strategy to prepare a Si@ZIF-8 architecture as the active anode materials in LIBs are evident from the improved electrochemical performance. With less than 10 wt % silicon loading, the specific capacity of Si@ZIF-8-700N reaches 1050 mA h g^{-1} at a current density of 50 mA g^{-1} (Figure 4a) and is maintained at 1020 mA h g^{-1} after 50 cycles, which is much higher than the capacity of ZIF-8 pyrolyzed at the same temperature (see Figure S6 in the Supporting Information). This result is also superior to that of pyrolyzed-ZIF-8 coated by chitosan.[10] Compared with the carbonized sample, the PXRD pattern and the FT-IR spectrum of bare electrode remain unchanged after galvanostatic cycling. The results demonstrate that the electrode composition did not change much under charge and discharge states (see Figure S10 in the Supporting Information). For the subsequent cycle-life performance, the Coulombic efficiency appears to level off immediately and remains constant at 99%, indicating that the SEI layer formed in the first cycle is fairly stable.[23] For the pure Si nanoparticles, the capacity dramatically decreases from 2200 to 100 mA h g^{-1} after 8 cycles, exhibiting a severe capacity loss of ~96% (see Figure S6 in the Supporting Information). By contrast, the cycling stability of Si@ZIF-8-700N is greatly improved. The long cycling performance is shown in Figure 4f. A high reversible capacity of 830 mA h g^{-1} at a current density of 200 mA g^{-1} is retained after 500 cycles. As shown in the galvanostatic charge/discharge curve (Figure 4b), the discharge plateau is below 1.0 V, which is effective and significant as the anode materials for the practical application for larger potential difference and power density. The stable cycling performance is further confirmed by the cyclic voltammetry (Figure 4c). Most of the lithiation potentials are below 1.0 V, consistent with the capacity-voltage profiles in Figure 4b. The two oxidation peaks at 0.32 and 0.53 V can be clearly attributed to the delithiation of Si,[24] and the peaks at 1.2 V could be attributed to the delithiation of Zn(II). The cyclic voltammetry of the first 3 cycles is shown in Figure S12 in the Supporting Information, we can find the SEI layer is formed during the first discharge process. As shown in Figure 3b, both of the plateau and the discharge capacity (1250 mAh g^{-1}) in the first cycle are quite different from those in the fifth cycle (discharge capacity: 1050 mAh g^{-1}). These differences in the voltage profiles as well as in the CV profiles can be attributed to the formation of SEI film on the surfaces of particles in the first discharge process. AC impedances are shown in Nyquist plots for Si@ZIF-8-700N and the nano Si powder (Figure 4e). The impedance of Si@ZIF-8-700N associated with the charge-transfer resistance is lower than that of the nano Si powder. Nyquist plots for ZIF-8-700N after four cycles are shown in Figure S9 in the Supporting Information; the impedance is similar to that of Si@ZIF-8-700N. The partially graphitic carbon layer yielded at 700 °C contributed significantly to the conductivity as a result of the sufficient thermal treatment of aromatic precursor, as shown in the HRTEM image (Figure 3e). We also checked the performance of Si@ZIF-8 nanocomposites. Because of the nonconducting property of Si@ZIF-8, the capacity could not be brought out (see Figure S11 in the Supporting Information).

To further examine the cycling stability and rate capacity of the materials, we performed the discharge and charge of the batteries at various current densities (Figure 4d). It can be found that the discharge capacity remains at 870, 800, 700, 520, and 300 mA h g^{-1} at a rate of 200, 400, 800, 1600, and 3200 mA g^{-1}, respectively. Remarkably, after the current density was switched back to 50 mA g^{-1}, the electrode can fully recover its capacity back to about 1050 mA h g^{-1} without any decay. The slight increase of the discharge capacity may attribute to part of the lithium ion remaining in the electrodes under larger current densities. It should be noted that the capacity of Si@ZIF-8-700N can be contributed to by Zn(II), Si, amorphous carbon, and nitrogen, so the voltage window was chosen between 0.02 and 3 V. The uniform distribution of Zn(II) and N-doped carbon facilitates the lithiation and delithiation process of Si particles and prevent volume expansion. ZIF-8-700 can be considered as aggregates of large amounts of graphene particles and Zn(II) analogues, both of which can contribute high capacity to the anode materials.[7,25,26] Therefore, although the content of Si is only 7.3%, the capacity of Si@ZIF-8-700N can reach as high as 1050 mAh g^{-1}. The double amount of Si added showed inferior electrochemical performance. The results show that the capacity drops rapidly during cycling, which demonstrates that the formation of crystalline framework is important for enhancing the cycle life (Figure S7 in the Supporting Information).

In summary, we have demonstrated an effective one-pot route to synthesize Si@ZIF-8 nanocrystals by in situ coating of MOF layers on the surface of Si particles. The pyrolyzed composite shows an improved specific capacity of 1050 mA h g^{-1}, lower impedance and impressive cycling stability. By virtue of the general and facile synthetic approach and outstanding electrochemical performance, this work may shed light on the future research in preparation of anode materials with enhanced performance through MOF-coated Si for practical energy applications. Although a modicum of Si was used in our materials, the performance of the lithium-ion battery already shows a remarkable improvement. Further research on increasing the quantity of Si and the lithium storage capacity is still in process and the results will be reported soon.

■ ASSOCIATED CONTENT

Ⓢ Supporting Information

Details of experiments and additional figures as described in the text. This material is available free of charge via the Internet at http://pubs.acs.org.

■ AUTHOR INFORMATION

Corresponding Author

*E-mail: bowang@bit.edu.cn.

Author Contributions

⊥Y.H. and P.Q. contributed equally.

Notes

The authors declare no competing financial interest.

DOI: 10.1021/am5081937
ACS Appl. Mater. Interfaces 2015, 7, 2178−2182

■ ACKNOWLEDGMENTS

This work was financially supported by the 973 Program 2013CB834704; Provincial Key Project of China (Grant 7131253); the National Natural Science Foundation of China (Grants 21471018, 21404010, 21201018); 1000 Plan (Youth).

■ REFERENCES

(1) Tarascon, J. M.; Armand, M. Issues and Challenges Facing Rechargeable Lithium Batteries. *Nature* **2001**, *414*, 359−367.
(2) Yang, Y.; Zheng, G.; Cui, Y. Nanostructured Sulfur Cathodes. *Chem. Soc. Rev.* **2013**, *42*, 3018−3032.
(3) Furukawa, H.; Cordova, K. E.; O'Keeffe, M.; Yaghi, O. M. The Chemistry and Applications of Metal-Organic Frameworks. *Science* **2013**, *341*, 974−988.
(4) Liu, B.; Shioyama, H.; Jiang, H. L.; Zhang, X. B.; Xu, Q. Metal-Organic Framework (MOF) as a Template for Syntheses of Nanoporous Carbons as Electrode Materials for Supercapacitor. *Carbon* **2010**, *48*, 456−463.
(5) Chapman, K. W.; Sava, D. F.; Halder, G. J.; Chupas, P. J.; Nenoff, T. M. Trapping Guests within a Nanoporous Metal-Organic Framework through Pressure-Induced Amorphization. *J. Am. Chem. Soc.* **2011**, *133*, 18583−18585.
(6) Xu, X.; Cao, R.; Jeong, S.; Cho, J. Spindle-like Mesoporous alpha-Fe_2O_3 Anode Material Prepared from MOF Template for High-Rate Lithium Batteries. *Nano Lett.* **2012**, *12*, 4988−4991.
(7) Yang, S. J.; Nam, S.; Kim, T.; Im, J. H.; Jung, H.; Kang, J. H.; Wi, S.; Park, B.; Park, C. R. Preparation and Exceptional Lithium Anodic Performance of Porous Carbon-coated ZnO Quantum Dots Derived from a Metal-Organic Framework. *J. Am. Chem. Soc.* **2013**, *135*, 7394−7397.
(8) Banerjee, A.; Singh, U.; Aravindan, V.; Srinivasan, M.; Ogale, S. Synthesis of CuO Nanostructures from Cu-Based Metal Organic Framework (MOF-199) for Application as Anode for Li-Ion Batteries. *Nano Energy* **2013**, *2*, 1158−1163.
(9) Wu, Y.; Wei, Y.; Wang, J. P.; Jiang, K. L.; Fan, S. S. Conformal Fe_3O_4 Sheath on Aligned Carbon Nanotube Scaffolds as High-Performance Anodes for Lithium Ion Batteries. *Nano Lett.* **2013**, *13*, 818−823.
(10) Han, Y.; Qi, P.; Li, S.; Feng, X.; Zhou, J.; Li, H.; Su, S.; Li, X.; Wang, B. A Novel Anode Material Derived from Organic-Coated ZIF-8 Nanocomposites with High Performance in Lithium Ion Batteries. *Chem. Commun.* **2014**, *50*, 8057−8060.
(11) Demir-Cakan, R.; Morcrette, M.; Nouar, F.; Davoisne, C.; Devic, T.; Gonbeau, D.; Dominko, R.; Serre, C.; Ferey, G.; Tarascon, J. M. Cathode Composites for Li-S Batteries via the Use of Oxygenated Porous Architectures. *J. Am. Chem. Soc.* **2011**, *133*, 16154−16160.
(12) Zhou, J.; Li, R.; Fan, X.; Chen, Y.; Han, R.; Li, W.; Zheng, J.; Wang, B.; Li, X. Rational Design of a Metal−Organic Framework Host for Sulfur Storage in Fast, Long-Cycle Li−S Batteries. *Energy Environ. Sci.* **2014**, *7*, 2715−2724.
(13) Chan, C. K.; Peng, H. L.; Liu, G.; McIlwrath, K.; Zhang, X. F.; Huggins, R. A.; Cui, Y. High-Performance Lithium Battery Anodes Using Silicon Nanowires. *Nat. Nanotechnol.* **2008**, *3*, 31−35.
(14) Kasavajjula, U.; Wang, C. S.; Appleby, A. J. Nano- and Bulk-Silicon-Based Insertion Anodes for Lithium-Ion Secondary Cells. *J. Power Sources* **2007**, *163*, 1003−1039.
(15) Su, X.; Wu, Q. L.; Li, J. C.; Xiao, X. C.; Lott, A.; Lu, W. Q.; Sheldon, B. W.; Wu, J. Silicon-Based Nanomaterials for Lithium-Ion Batteries: A Review. *Adv. Energy Mater.* **2014**, *4*, 1300882.
(16) Gu, M.; Li, Y.; Li, X. L.; Hu, S. Y.; Zhang, X. W.; Xu, W.; Thevuthasan, S.; Baer, D. R.; Zhang, J. G.; Liu, J.; Wang, C. M. In Situ TEM Study of Lithiation Behavior of Silicon Nanoparticles Attached to and Embedded in a Carbon Matrix. *ACS Nano* **2012**, *6*, 8439−8447.
(17) Riley, L. A.; Cavanagh, A. S.; George, S. M.; Jung, Y. S.; Yan, Y. F.; Lee, S. H.; Dillon, A. C. Conformal Surface Coatings to Enable High Volume Expansion Li-Ion Anode Materials. *ChemPhysChem* **2010**, *11*, 2124−2130.
(18) Dake, L. S.; Baer, D. R.; Zachara, J. M. Auger Parameter Measurements of Zinc-Compounds Relevant to Zinc Transport in the Environment. *Surf. Interface Anal.* **1989**, *14*, 71−75.
(19) Nefedov, V. I.; Salyn, Y. V.; Domashevskaya, E. P.; Ugai, Y. A.; Terekhov, V. A. A Study by XPS and XRS of the Participation in Chemical Bonding of the 3d Electrons of Copper, Zinc and Gallium. *J. Electron Spectrosc. Relat. Phenom.* **1975**, *6*, 231−238.
(20) Guo, Y. G.; Hu, J. S.; Wan, L. J. Nanostructured Materials for Electrochemical Energy Conversion and Storage Devices. *Adv. Mater.* **2008**, *20*, 4384−4384.
(21) Li, P. Y.; Deng, J. C.; Li, Y.; Liang, W.; Wang, K.; Kang, L. T.; Zeng, S. Z.; Yin, S. H.; Zhao, Z. G.; Liu, X. G.; Yang, Y. Z.; Gao, F. One-Step Solution Combustion Synthesis of Fe_2O_3/C Nano-Composites as Anode Materials for Lithium Ion Batteries. *J. Alloy. Compd.* **2014**, *590*, 318−323.
(22) Bresser, D.; Paillard, E.; Kloepsch, R.; Krueger, S.; Fiedler, M.; Schmitz, R.; Baither, D.; Winter, M.; Passerini, S. Carbon Coated $ZnFe_2O_4$ Nanoparticles for Advanced Lithium-Ion Anodes. *Adv. Energy Mater.* **2013**, *3*, 513−523.
(23) Wu, Z. S.; Ren, W. C.; Wen, L.; Gao, L. B.; Zhao, J. P.; Chen, Z. P.; Zhou, G. M.; Li, F.; Cheng, H. M. Graphene Anchored with Co3O4 Nanoparticles as Anode of Lithium Ion Batteries with Enhanced Reversible Capacity and Cyclic Performance. *ACS Nano* **2010**, *4*, 3187−3194.
(24) Zamfir, M. R.; Nguyen, H. T.; Moyen, E.; Lee, Y. H.; Pribat, D. Silicon Nanowires for Li-Based Battery Anodes: A Review. *J. Mater. Chem. A* **2013**, *1*, 9566−9586.
(25) Wu, Z. S.; Ren, W. C.; Xu, L.; Li, F.; Cheng, H. M. Doped Graphene Sheets as Anode Materials with Superhigh Rate and Large Capacity for Lithium Ion Batteries. *ACS Nano* **2011**, *5*, 5463−5471.
(26) Zheng, F.; Yang, Y.; Chen, Q. High Lithium Anodic Performance of Highly Nitrogen-Doped Porous Carbon Prepared from a Metal-Organic Framework. *Nat. Commun.* **2014**, *5*, 5261−5270.

DOI: 10.1021/am5081937
ACS Appl. Mater. Interfaces 2015, 7, 2178−2182